# Differential limit on the extremely-high-energy cosmic neutrino flux in the presence of astrophysical background from nine years of IceCube data

M. G. Aartsen,[16] M. Ackermann,[52] J. Adams,[16] J. A. Aguilar,[12] M. Ahlers,[20] M. Ahrens,[44] I. Al Samarai,[25] D. Altmann,[24] K. Andeen,[34] T. Anderson,[49] I. Ansseau,[12] G. Anton,[24] C. Argüelles,[14] J. Auffenberg,[1] S. Axani,[14] P. Backes,[1] H. Bagherpour,[16] X. Bai,[41] A. Barbano,[25] J. P. Barron,[23] S. W. Barwick,[27] V. Baum,[33] R. Bay,[8] J. J. Beatty,[18,19] J. Becker Tjus,[11] K.-H. Becker,[51] S. BenZvi,[43] D. Berley,[17] E. Bernardini,[52] D. Z. Besson,[28] G. Binder,[9,8] D. Bindig,[51] E. Blaufuss,[17] S. Blot,[52] C. Bohm,[44] M. Börner,[21] F. Bos,[11] S. Böser,[33] O. Botner,[50] E. Bourbeau,[20] J. Bourbeau,[32] F. Bradascio,[52] J. Braun,[32] M. Brenzke,[1] H.-P. Bretz,[52] S. Bron,[25] J. Brostean-Kaiser,[52] A. Burgman,[50] R. S. Busse,[32] T. Carver,[25] E. Cheung,[17] D. Chirkin,[32] A. Christov,[25] K. Clark,[29] L. Classen,[36] G. H. Collin,[14] J. M. Conrad,[14] P. Coppin,[13] P. Correa,[13] D. F. Cowen,[49,48] R. Cross,[43] P. Dave,[6] M. Day,[32] J. P. A. M. de André,[22] C. De Clercq,[13] J. J. DeLaunay,[49] H. Dembinski,[37] K. Deoskar,[44] S. De Ridder,[26] P. Desiati,[32] K. D. de Vries,[13] G. de Wasseige,[13] M. de With,[10] T. DeYoung,[22] J. C. Díaz-Vélez,[32] V. di Lorenzo,[33] H. Dujmovic,[46] J. P. Dumm,[44] M. Dunkman,[49] E. Dvorak,[41] B. Eberhardt,[33] T. Ehrhardt,[33] B. Eichmann,[11] P. Eller,[49] P. A. Evenson,[37] S. Fahey,[32] A. R. Fazely,[7] J. Felde,[17] K. Filimonov,[8] C. Finley,[44] S. Flis,[44] A. Franckowiak,[52] E. Friedman,[17] A. Fritz,[33] T. K. Gaisser,[37] J. Gallagher,[31] E. Ganster,[1] L. Gerhardt,[9] K. Ghorbani,[32] W. Giang,[23] T. Glauch,[35] T. Glüsenkamp,[24] A. Goldschmidt,[9] J. G. Gonzalez,[37] D. Grant,[23] Z. Griffith,[32] C. Haack,[1] A. Hallgren,[50] L. Halve,[1] F. Halzen,[32] K. Hanson,[32] D. Hebecker,[10] D. Heereman,[12] K. Helbing,[51] R. Hellauer,[17] S. Hickford,[51] J. Hignight,[22] G. C. Hill,[2] K. D. Hoffman,[17] R. Hoffmann,[51] T. Hoinka,[21] B. Hokanson-Fasig,[32] K. Hoshina,[32,*] F. Huang,[49] M. Huber,[35] K. Hultqvist,[44] M. Hünnefeld,[21] R. Hussain,[32] S. In,[46] N. Iovine,[12] A. Ishihara,[15] E. Jacobi,[52] G. S. Japaridze,[5] M. Jeong,[46] K. Jero,[32] B. J. P. Jones,[4] P. Kalaczynski,[1] W. Kang,[46] A. Kappes,[36] D. Kappesser,[33] T. Karg,[52] A. Karle,[32] U. Katz,[24] M. Kauer,[32] A. Keivani,[49] J. L. Kelley,[32] A. Kheirandish,[32] J. Kim,[46] T. Kintscher,[52] J. Kiryluk,[45] T. Kittler,[24] S. R. Klein,[9,8] R. Koirala,[37] H. Kolanoski,[10] L. Köpke,[33] C. Kopper,[23] S. Kopper,[47] J. P. Koschinsky,[1] D. J. Koskinen,[20] M. Kowalski,[10,52] K. Krings,[35] M. Kroll,[11] G. Krückl,[33] S. Kunwar,[52] N. Kurahashi,[40] A. Kyriacou,[2] M. Labare,[26] J. L. Lanfranchi,[49] M. J. Larson,[20] F. Lauber,[51] K. Leonard,[32] M. Leuermann,[1] Q. R. Liu,[32] E. Lohfink,[33] C. J. Lozano Mariscal,[36] L. Lu,[15] J. Lünemann,[13] W. Luszczak,[32] J. Madsen,[42] G. Maggi,[13] K. B. M. Mahn,[22] Y. Makino,[15] S. Mancina,[32] I. C. Mariş,[12] R. Maruyama,[38] K. Mase,[15] R. Maunu,[17] K. Meagher,[12] M. Medici,[20] M. Meier,[21] T. Menne,[21] G. Merino,[32] T. Meures,[12] S. Miarecki,[9,8] J. Micallef,[22] G. Momenté,[33] T. Montaruli,[25] R. W. Moore,[23] M. Moulai,[14] R. Nagai,[15] R. Nahnhauer,[52] P. Nakarmi,[47] U. Naumann,[51] G. Neer,[22] H. Niederhausen,[45] S. C. Nowicki,[23] D. R. Nygren,[9] A. Obertacke Pollmann,[51] A. Olivas,[17] A. O'Murchadha,[12] E. O'Sullivan,[44] T. Palczewski,[9,8] H. Pandya,[37] D. V. Pankova,[49] P. Peiffer,[33] J. A. Pepper,[47] C. Pérez de los Heros,[50] D. Pieloth,[21] E. Pinat,[12] A. Pizzuto,[32] M. Plum,[34] P. B. Price,[8] G. T. Przybylski,[9] C. Raab,[12] L. Rädel,[1] M. Rameez,[20] L. Rauch,[52] K. Rawlins,[3] I. C. Rea,[35] R. Reimann,[1] B. Relethford,[40] G. Renzi,[12] E. Resconi,[35] W. Rhode,[21] M. Richman,[40] S. Robertson,[2] M. Rongen,[1] C. Rott,[46] T. Ruhe,[21] D. Ryckbosch,[26] D. Rysewyk,[22] I. Safa,[32] S. E. Sanchez Herrera,[23] A. Sandrock,[21] J. Sandroos,[33] M. Santander,[47] S. Sarkar,[20,39] S. Sarkar,[23] K. Satalecka,[52] M. Schaufel,[1] P. Schlunder,[21] T. Schmidt,[17] A. Schneider,[32] S. Schoenen,[1] S. Schöneberg,[11] L. Schumacher,[1] S. Sclafani,[40] D. Seckel,[37] S. Seunarine,[42] J. Soedingrekso,[21] D. Soldin,[37] M. Song,[17] G. M. Spiczak,[42] C. Spiering,[52] J. Stachurska,[52] M. Stamatikos,[18] T. Stanev,[37] A. Stasik,[52] R. Stein,[52] J. Stettner,[1] A. Steuer,[33] T. Stezelberger,[9] R. G. Stokstad,[9] A. Stößl,[15] N. L. Strotjohann,[52] T. Stuttard,[20] G. W. Sullivan,[17] M. Sutherland,[18] I. Taboada,[6] F. Tenholt,[11] S. Ter-Antonyan,[7] A. Terliuk,[52] S. Tilav,[37] P. A. Toale,[47] M. N. Tobin,[32] C. Tönnis,[46] S. Toscano,[13] D. Tosi,[32] M. Tselengidou,[24] C. F. Tung,[6] A. Turcati,[35] C. F. Turley,[49] B. Ty,[32] E. Unger,[50] M. Usner,[52] J. Vandenbroucke,[32] W. Van Driessche,[26] D. van Eijk,[32] N. van Eijndhoven,[13] S. Vanheule,[26] J. van Santen,[52] M. Vraeghe,[26] C. Walck,[44] A. Wallace,[2] M. Wallraff,[1] F. D. Wandler,[23] N. Wandkowsky,[32] T. B. Watson,[4] A. Waza,[1] C. Weaver,[23] M. J. Weiss,[49] C. Wendt,[32] J. Werthebach,[32] S. Westerhoff,[32] B. J. Whelan,[2] N. Whitehorn,[30] K. Wiebe,[33] C. H. Wiebusch,[1] L. Wille,[32] D. R. Williams,[47] L. Wills,[40] M. Wolf,[35] J. Wood,[32] T. R. Wood,[23] E. Woolsey,[23] K. Woschnagg,[8] G. Wrede,[24] D. L. Xu,[32] X. W. Xu,[7] Y. Xu,[45] J. P. Yanez,[23] G. Yodh,[27] S. Yoshida,[15] and T. Yuan[32]

(IceCube Collaboration)[†]

[1]*III. Physikalisches Institut, RWTH Aachen University, D-52056 Aachen, Germany*
[2]*Department of Physics, University of Adelaide, Adelaide 5005, Australia*
[3]*Department of Physics and Astronomy, University of Alaska Anchorage, 3211 Providence Dr., Anchorage, Alaska 99508, USA*

 

[4]Department of Physics, University of Texas at Arlington, 502 Yates St., Science Hall Rm 108, Box 19059, Arlington, Texas 76019, USA
[5]CTSPS, Clark-Atlanta University, Atlanta, Georgia 30314, USA
[6]School of Physics and Center for Relativistic Astrophysics, Georgia Institute of Technology, Atlanta, Georgia 30332, USA
[7]Department of Physics, Southern University, Baton Rouge, Louisiana 70813, USA
[8]Department of Physics, University of California, Berkeley, California 94720, USA
[9]Lawrence Berkeley National Laboratory, Berkeley, California 94720, USA
[10]Institut für Physik, Humboldt-Universität zu Berlin, D-12489 Berlin, Germany
[11]Fakultät für Physik & Astronomie, Ruhr-Universität Bochum, D-44780 Bochum, Germany
[12]Université Libre de Bruxelles, Science Faculty CP230, B-1050 Brussels, Belgium
[13]Vrije Universiteit Brussel (VUB), Dienst ELEM, B-1050 Brussels, Belgium
[14]Department of Physics, Massachusetts Institute of Technology, Cambridge, Massachusetts 02139, USA
[15]Department of Physics and Institute for Global Prominent Research, Chiba University, Chiba 263-8522, Japan
[16]Department of Physics and Astronomy, University of Canterbury, Private Bag 4800, Christchurch, New Zealand
[17]Department of Physics, University of Maryland, College Park, Maryland 20742, USA
[18]Department of Physics and Center for Cosmology and Astro-Particle Physics, Ohio State University, Columbus, Ohio 43210, USA
[19]Department of Astronomy, Ohio State University, Columbus, Ohio 43210, USA
[20]Niels Bohr Institute, University of Copenhagen, DK-2100 Copenhagen, Denmark
[21]Department of Physics, TU Dortmund University, D-44221 Dortmund, Germany
[22]Department of Physics and Astronomy, Michigan State University, East Lansing, Michigan 48824, USA
[23]Department of Physics, University of Alberta, Edmonton, Alberta, Canada T6G 2E1
[24]Erlangen Centre for Astroparticle Physics, Friedrich-Alexander-Universität Erlangen-Nürnberg, D-91058 Erlangen, Germany
[25]Département de physique nucléaire et corpusculaire, Université de Genève, CH-1211 Genève, Switzerland
[26]Department of Physics and Astronomy, University of Gent, B-9000 Gent, Belgium
[27]Department of Physics and Astronomy, University of California, Irvine, California 92697, USA
[28]Department of Physics and Astronomy, University of Kansas, Lawrence, Kansas 66045, USA
[29]SNOLAB, 1039 Regional Road 24, Creighton Mine 9, Lively, Ontario, Canada P3Y 1N2
[30]Department of Physics and Astronomy, UCLA, Los Angeles, California 90095, USA
[31]Department of Astronomy, University of Wisconsin, Madison, Wisconsin 53706, USA
[32]Department of Physics and Wisconsin IceCube Particle Astrophysics Center, University of Wisconsin, Madison, Wisconsin 53706, USA
[33]Institute of Physics, University of Mainz, Staudinger Weg 7, D-55099 Mainz, Germany
[34]Department of Physics, Marquette University, Milwaukee, Wisconsin 53201, USA
[35]Physik-department, Technische Universität München, D-85748 Garching, Germany
[36]Institut für Kernphysik, Westfälische Wilhelms-Universität Münster, D-48149 Münster, Germany
[37]Bartol Research Institute and Department of Physics and Astronomy, University of Delaware, Newark, Delaware 19716, USA
[38]Department of Physics, Yale University, New Haven, Connecticut 06520, USA
[39]Department of Physics, University of Oxford, 1 Keble Road, Oxford OX1 3NP, United Kingdom
[40]Department of Physics, Drexel University, 3141 Chestnut Street, Philadelphia, Pennsylvania 19104, USA
[41]Physics Department, South Dakota School of Mines and Technology, Rapid City, South Dakota 57701, USA
[42]Department of Physics, University of Wisconsin, River Falls, Wisconsin 54022, USA
[43]Department of Physics and Astronomy, University of Rochester, Rochester, New York 14627, USA
[44]Oskar Klein Centre and Department of Physics, Stockholm University, SE-10691 Stockholm, Sweden
[45]Department of Physics and Astronomy, Stony Brook University, Stony Brook, New York 11794-3800, USA
[46]Department of Physics, Sungkyunkwan University, Suwon 440-746, Korea
[47]Department of Physics and Astronomy, University of Alabama, Tuscaloosa, Alabama 35487, USA

[48]Department of Astronomy and Astrophysics, Pennsylvania State University, University Park, Pennsylvania 16802, USA
[49]Department of Physics, Pennsylvania State University, University Park, Pennsylvania 16802, USA
[50]Department of Physics and Astronomy, Uppsala University, Box 516, S-75120 Uppsala, Sweden
[51]Department of Physics, University of Wuppertal, D-42119 Wuppertal, Germany
[52]DESY, D-15738 Zeuthen, Germany

(Received 4 July 2018; published 12 September 2018)

We report a quasidifferential upper limit on the extremely-high-energy (EHE) neutrino flux above $5 \times 10^6$ GeV based on an analysis of nine years of IceCube data. The astrophysical neutrino flux measured by IceCube extends to PeV energies, and it is a background flux when searching for an independent signal flux at higher energies, such as the cosmogenic neutrino signal. We have developed a new method to place robust limits on the EHE neutrino flux in the presence of an astrophysical background, whose spectrum has yet to be understood with high precision at PeV energies. A distinct event with a deposited energy above $10^6$ GeV was found in the new two-year sample, in addition to the one event previously found in the seven-year EHE neutrino search. These two events represent a neutrino flux that is incompatible with predictions for a cosmogenic neutrino flux and are considered to be an astrophysical background in the current study. The obtained limit is the most stringent to date in the energy range between $5 \times 10^6$ and $2 \times 10^{10}$ GeV. This result constrains neutrino models predicting a three-flavor neutrino flux of $E_\nu^2 \phi_{\nu_e+\nu_\mu+\nu_\tau} \simeq 2 \times 10^{-8}$ GeV/cm$^2$ sec sr at $10^9$ GeV. A significant part of the parameter space for EHE neutrino production scenarios assuming a proton-dominated composition of ultra-high-energy cosmic rays is disfavored independently of uncertain models of the extragalactic background light which previous IceCube constraints partially relied on.

DOI: 10.1103/PhysRevD.98.062003

## I. INTRODUCTION

The origin of ultra-high-energy cosmic rays (UHECRs; cosmic rays with energies greater than about $10^{18}$ eV) is among the long-standing questions in astrophysics. Recent measurements indicate that they originate from extragalactic sources [1]. Secondary extremely-high-energy (EHE) neutrinos produced by UHECR interactions with background radiation provide an alternative and promising indicator of UHECR sources as neutrinos propagate cosmological distances without interaction or deflection by magnetic fields. A series of EHE neutrino searches have been conducted [2–5]; however, cosmogenic neutrinos induced by the Greisen-Zatsepin-Kuzmin (GZK) mechanism [6] have not been detected. Because the cosmogenic neutrino rates strongly depend on the UHECR source evolution function that characterizes the source classes [7–9], recent limits on the EHE neutrino flux by the IceCube Neutrino Observatory have provided a unique constraint on UHECR sources. The aforementioned limits published by IceCube [5] and subsequently reported by Auger [10] indicate that objects with a cosmological evolution stronger than the star formation rate (SFR) are disfavored as UHECR sources, if the UHECRs are proton-dominated.

A differential limit is an effective way to characterize the energy dependence of an experiment's sensitivity. As each experiment is sensitive to neutrinos of different energy, a model-dependent constraint does not indicate which energy region contributes most to bounding a given model. In the case of the null observation, Anchordoqui *et al.* [11] proposed setting a quasidifferential limit:

$$\phi^{\mathrm{UL}}_{\nu_e+\nu_\mu+\nu_\tau}(E_\nu) = 3\frac{\mathrm{N}_{90}}{4\pi E_\nu T \log\, 10 \sum_{i=\nu_e,\nu_\mu,\nu_\tau} A_i^\nu(E_\nu)}, \qquad (1)$$

where $T$ is the observation time, $A_i^\nu$ is the $4\pi$-averaged neutrino effective area for a neutrino flavor $i$, and $\mathrm{N}_{90}$ is the 90% C.L. upper limit on the number of events. The Feldman-Cousins method [12] sets $\mathrm{N}_{90} = 2.4$ for the case of negligible background. An equal flavor ratio of neutrino fluxes $\nu_e : \nu_\mu : \nu_\tau = 1:1:1$ at the Earth is assumed. This upper limit of Eq. (1) is equivalent to the limit on the normalization of neutrino fluxes following $E_\nu^{-1}$ with an interval of one decade.

This formula must be modified when neutrino event candidates are contained in the data sample. However, it is not clear what approach should be employed to incorporate detected events in the calculation of the differential limit. Muon neutrino events deposit an unmeasured fraction of their energy outside the instrument volume. Therefore, a

*Earthquake Research Institute, University of Tokyo, Bunkyo, Tokyo 113-0032, Japan.
†analysis@icecube.wisc.edu

large uncertainty in the measured muon neutrino energy cannot be avoided. The probability density function (PDF) of the observed neutrino energy thus depends on the as-yet unknown true neutrino energy spectrum. In the EHE neutrino analysis with IceCube published in 2013 [3], in which the first PeV events were detected in two years of data [13], the upper limit on the number of events $N_{90}$ in Eq. (1) was derived from the probability of finding $n$ ($n = 0, 1, 2, \ldots$) neutrino events in an interval of one decade: $[\log_{10}(E_\nu/\mathrm{GeV}) - 0.5, \log_{10}(E_\nu/\mathrm{GeV}) + 0.5]$. This probability was estimated using the PDF of the primary neutrino energy for each of the detected events, assuming the parent neutrino energy spectrum followed $E_\nu^{-2}$. However, the confidence coverage is not well defined in this approach as each of the Poisson upper limits at the 90% confidence level in the case of finding $n$ events are further weighted by the $n$ event detection Bayesian probability. Moreover, it does not fully consider the energy dependence of the background contamination.

In this paper, we present a complete frequentist approach to calculate the flux limits and update the constraints using a collection of IceCube data taken over nine years from April 2008 to May 2017. The data sample includes two additional years of IceCube data in addition to the seven-year sample used in the previous EHE analysis [5]. All signal selection criteria are the same as in the previous publication and described in Secs. II and III. The new approach using a nuisance parameter to represent the unknown astrophysical background and the method of p-value calculations using the Poisson-binned likelihood ratio are presented in Sec. IV. Last, the results and implications of the derived limits for explaining the origin of UHECRs are discussed in Sec. V.

## II. DATA AND SIMULATION

IceCube is a cubic-kilometer neutrino detector installed in the ice under the South Pole between depths of 1450 and 2450 m, forming a three-dimensional array of digital optical modules (DOMs) [14]. To form the detector, cable assemblies called strings were lowered into holes drilled vertically into the glacier ice with a horizontal spacing of approximately 125 m. The detector construction was completed in December 2010 and the observatory has been in full operation with 86 strings (IC86) since May 2011. During the construction period, it was partially operated with 40, 59, and 79 strings in 2008–2009, 2009–2010, and 2010–2011, respectively. The analysis described here is based on data taken from April 2008 to May 2017. The effective live time of the sample is 3142.5 days. The most recent two-year data sample provides approximately 30% more exposure than the previous EHE neutrino search [5].

There are two classes of atmospheric background events: atmospheric muon bundles and events generated by atmospheric neutrinos. They were simulated using the CORSIKA [15] package with the SIBYLL hadronic interaction model [16] and by the IceCube neutrino-generator program based on the ANIS code [17], respectively. Prompt atmospheric neutrinos from short-lived heavy meson decays were modeled following Ref. [18], which predicted a higher prompt neutrino flux than recent calculations [19], and represent a conservative background estimate. The EHE neutrino-induced events were simulated by the JULIET package [20], which provides the cosmogenic (GZK) signal simulation sample as well as simulations of the astrophysical *background* events, whose spectrum is assumed to be described by an unbroken power law in the relevant energy region. The detailed simulation procedure used in this work is described in Ref. [3].

## III. EVENT SELECTION

The EHE signal selection criteria remain the same as in the previous analysis [5]. The selection criteria were determined by following a blind analysis strategy, and the cut value optimization was carried out by looking at the simulated event samples with the experimental data blind, except for a 10% subset of experimental data used to validate the simulation. The backgrounds for the EHE neutrino search are atmospheric muon bundles and atmospheric neutrinos initiated in cosmic-ray air showers. As the EHE signal events deposit more energy in the form of Cherenkov light than the background, the total number of photoelectrons (NPE) recorded in an event is used as the main distinctive feature to eliminate the background. This basic algorithm was established in the EHE neutrino search based on two years of IceCube data [3].

The *Online EHE Filter* first selects events with an NPE greater than 1000 photoelectrons (p.e.). After removing DOM signals from coincident atmospheric muons and photomultiplier tube dark noise [3], the *Offline EHE Cut* selects candidate events by requesting at least 25 000 p.e. and more than 100 hit DOMs. The technical details such as the NPE extraction method and hit cleaning algorithm are fully described in Ref. [3]. The event direction of surviving events is reconstructed by the LineFit algorithm [21] that masks photon hits which have substantially different timing distributions from Cherenkov photons radiated by an EHE muon track [22].

The *Track Quality Cut* is then applied based on the LineFit goodness-of-fit parameter $\chi^2_{\mathrm{track}}/\mathrm{d.o.f.}$, which is a measure of the consistency with a track-like event topology. Track-like events (primarily from muons and EHE taus) generally yield smaller NPE than cascade-like events (primarily from electrons and hadrons) of the same energy as track-like events deposit only a small fraction of the parent neutrino energy within the detection volume. Consequently, we reduced the NPE threshold for track-like events and relative to the cascade-like events in the track quality cut:

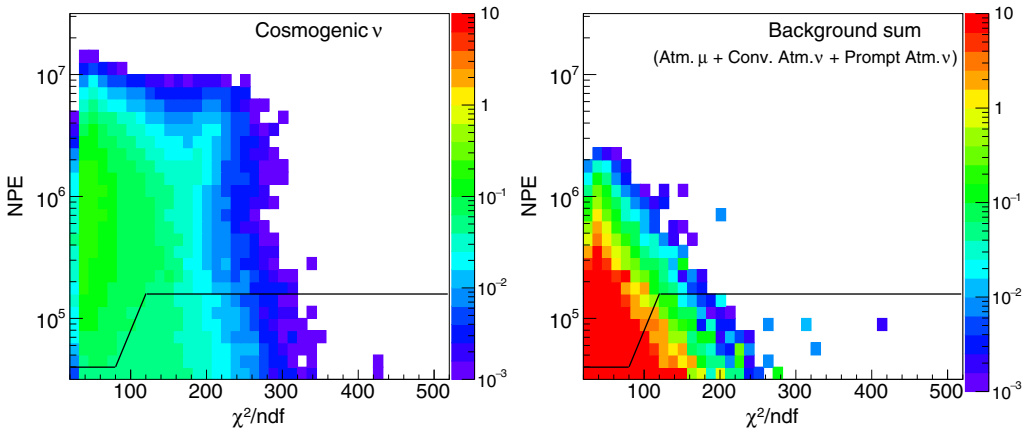


FIG. 1. Event count distributions before the track quality cut of the sample, including all three flavors of neutrinos as a function of NPE and $\chi^2_{\text{track}}/\text{d.o.f.}$ The colors indicate the expected number of events seen by the IceCube EHE neutrino analysis in the nine-year exposure. The solid line in each panel indicates the track quality selection criteria, where events above the lines are retained. Simulations of a cosmogenic (GZK) neutrino model [24] are shown in the left panel, and the background simulations of atmospheric muons, conventional atmospheric neutrinos, and prompt atmospheric neutrinos are shown in the right panel.

$$\log_{10}\text{NPE} \geq \begin{cases} 4.6 & (\frac{\chi^2_{\text{track}}}{\text{d.o.f.}} < 80), \\ 0.015(\frac{\chi^2_{\text{track}}}{\text{d.o.f.}} - 80) + 4.6 & \\ & (80 \leq \frac{\chi^2_{\text{track}}}{\text{d.o.f.}} < 120), \\ 5.2 & (120 \leq \frac{\chi^2_{\text{track}}}{\text{d.o.f.}}). \end{cases} \tag{2}$$

Figure 1 shows the signal and background event distributions as a function of $\chi^2_{\text{track}}/\text{d.o.f.}$ and NPE. The solid line represents the cut described by Eq. (2). Note that this selection criterion filters out the previously observed PeV energy neutrino-induced cascade events [13]. Muon track events dominate for $\chi^2_{\text{track}}/\text{d.o.f.} < 80$. A subsample of events that meets this $\chi^2_{\text{track}}$ condition is used for the EHE track alert system [23].

The final event selection cut is made based on the NPE and LineFit reconstructed zenith angle ($\cos\theta_{\text{LF}}$). A zenith angle-dependent NPE threshold is used to remove the atmospheric muon background in the downward-going region. The selection criteria in this *Muon Bundle Cut* are

$$\log_{10}\text{NPE} \geq \begin{cases} 4.6 & (\cos\theta_{\text{LF}} < 0.06), \\ 4.6 + 1.85\times & \\ \sqrt{1.0 - \left(\frac{1.0-\cos\theta_{\text{LF}}}{0.94}\right)^2} & (\cos\theta_{\text{LF}} \geq 0.06). \end{cases} \tag{3}$$

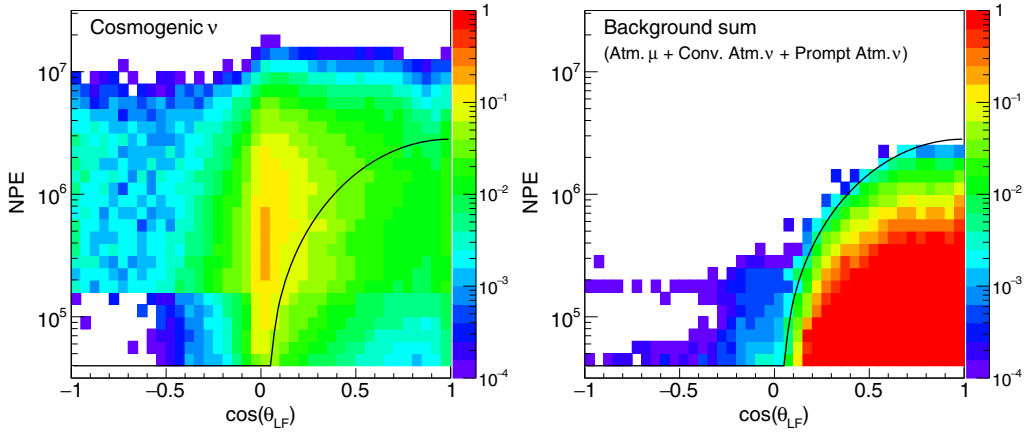


FIG. 2. Event count distributions before the muon bundle cut, including all three flavors of neutrinos as a function of NPE and $\cos(\theta_{\text{LF}})$. The colors indicate the expected number of events seen by the IceCube EHE neutrino analysis in the nine-year exposure. The solid line in each panel indicates the muon bundle selection criteria, where events above the lines are retained. The major sources of remaining background are rare high-energy atmospheric neutrinos and muons originating in UHECRs. Again, cosmogenic (GZK) neutrinos are shown in the left panel, while background simulations are shown in the right panel.

TABLE I. Rates and fractions of simulated data surviving by type as a function of event selection level applied with IC86 configuration. Efficiencies are calculated with respect to the online EHE filter.

| Cut level | Atmospheric muons number [Hz] | Atmospheric neutrinos number [Hz] | Signal cosmogenic neutrinos [24] fraction surviving (%) |
|---|---|---|---|
| Online EHE filter | 0.8 | $7.6 \times 10^{-6}$ | 100 |
| Offline EHE cut | $6.7 \times 10^{-4}$ | $1.0 \times 10^{-8}$ | 74 |
| Track quality cut | $1.6 \times 10^{-4}$ | $6.1 \times 10^{-10}$ | 61 |
| Muon bundle cut | $3.0 \times 10^{-10}$ | $3.6 \times 10^{-10}$ | 43 |

They are optimized for the cosmogenic neutrino model [24] with the least model rejection potential technique [25]. Figure 2 shows the signal and background event distributions as a function of $\cos\theta_{\mathrm{LF}}$ and $\log_{10}$ NPE. The muon bundle cut criteria [Eq. (3)] are shown by the solid line in the figure.

The passing rates in each stage of the cuts with the IC86 configuration are described in Table I. The expected number of atmospheric background events in the nine-year data sample passing the selection criteria is 0.085. The expected event rate from a cosmogenic model [24] assuming the UHECR primaries to be dominated by protons is 3.7–7.0. This model [24] takes into account Fermi-LAT bounds on the $\gamma$-ray background generated by cascading of the high-energy photons and electrons which are also produced in the GZK interactions. The range of the predicted cosmogenic neutrino flux (see Table III) corresponds to different choices of the "crossover" energy (1, 3 or 10 EeV) above which the extragalactic UHECR dominates over the Galactic component. The astrophysical neutrino flux [26] can extend to the EHE region, and will yield an astrophysical background with rates of $\lesssim$6 events in the nine-year analysis sample, depending on its spectral shape.

## IV. BINNED POISSON LIKELIHOOD METHOD

### A. General model test

In this analysis, observations are tested against theoretical models using a binned Poisson likelihood method, which is defined as the product of the Poisson probabilities over all zenith and energy bins as

$$L(\lambda) = \prod_{i,j} P(n_{i,j}; \lambda\mu_{i,j}^{\mathrm{SIG}} + \mu_{i,j}^{\mathrm{BG}}), \tag{4}$$

where $P(n;\mu)$ is a Poisson PDF of observing $n$ events with the expectation of $\mu$ events. $\mu_{i,j}^{\mathrm{SIG}}$ and $\mu_{i,j}^{\mathrm{BG}}$ are the mean number of the signal and background (atmospheric neutrino and muons) events, respectively, as functions of the cosine of the zenith angle (represented by bin $i$) and logarithm of an energy proxy defined below (bin $j$). The data are binned in 42 zenith bins, and 32 energy proxy bins for this analysis. The multiplier for a signal model, $\lambda$, can be varied in the test statistic construction. $\lambda = 1$ represents the predicted signal model strength. Figure 3 presents some example event distributions. The energy proxy used here is

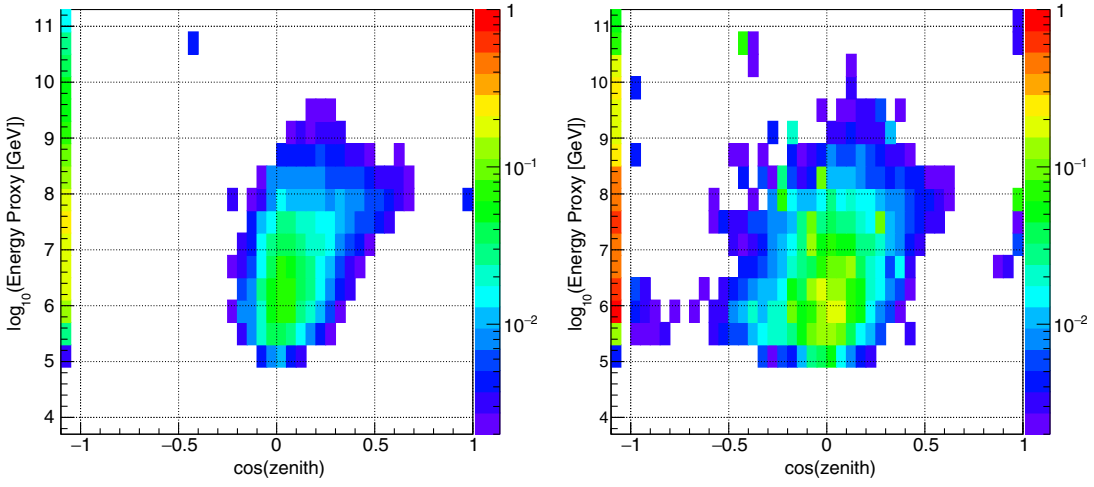


FIG. 3. Event distributions as functions of the energy proxy and cosine of the reconstructed zenith angle for simulations of the (left panel) cosmogenic (GZK) model [24] and (right panel) astrophysical neutrino model with a $E_\nu^{-2}$ spectrum with an intensity of $E_\nu^2\phi_{\nu_e+\nu_\mu+\nu_\tau} = 10^{-8}$ GeV/cm$^2$ sec sr. The colors indicate the expected number of events seen by the IceCube EHE neutrino analysis based on the data collected over nine years. Rare misreconstructed events are distributed in the unphysical region of the energy-direction parameter space and included in the figure. Events classified in the non-track-like category are plotted in the bins of cos(zenith) $= -1.1$.

an energy deposition reconstruction that employs a single-muon hypothesis with a series of stochastic energy losses from cascades along the muon track [27]. In the present analysis, the energy deposition reconstruction is specifically optimized to minimize the number of failed fits so that no additional fit quality selections are required to obtain the event distributions. The energy reconstruction method also shows reasonable performance for cascade-like events. The resulting resolution of the energy proxy is approximately 0.8 decade for through-going tracks, and 0.5 decade for contained cascade-like events. Though the stochastic nature of the EHE track energy loss profile broadens the resolution, this energy deposition measure offers sufficient correlations with neutrino energies to perform statistical tests on a given model flux. The zenith angle, $\theta$, used here is provided by the single photoelectron log-likelihood fit [28] based on the track hypothesis. Events with the log-likelihood values inconsistent with the track hypothesis are categorized in the *non-track-like* category. Directional information for non-track-like events is not used in the analysis.

A model test is performed by comparing the model hypothesis of $\lambda = 1$ against the alternative hypothesis $\lambda \neq 1$. The test statistic is the log-likelihood ratio:

$$\Lambda = \log \frac{L(\hat{\lambda})}{L(\lambda = 1)}, \tag{5}$$

where $\hat{\lambda}$ is the multiplier that maximizes the Poisson likelihood $L$ by floating $\lambda$ between zero and infinity. An ensemble of pseudoexperiments under the model hypothesis is used to produce a PDF of the test statistic $\Lambda$. The p-value for a given model of cosmic neutrinos is then calculated from the PDF by the frequency where $\Lambda$ is larger than the $\Lambda$ observed. A test of the atmospheric background only hypothesis is also conducted, where $\lambda = 0$.

### B. Model comparison

The binned Poisson likelihood introduced for the cosmogenic (GZK) model ($L_{\rm GZK}$) and power-law model ($L_{\rm power}$) can be written as

$$\begin{aligned} L_{\rm GZK}(\lambda_{\rm GZK}) &= \prod_{i,j} P(n_{i,j}; \lambda_{\rm GZK}\mu_{i,j}^{\rm GZK} + \mu_{i,j}^{\rm BG}), \\ L_{\rm power}(\lambda_\alpha) &= \prod_{i,j} P(n_{i,j}; \lambda_\alpha \mu_{i,j}^{\alpha} + \mu_{i,j}^{\rm BG}), \end{aligned} \tag{6}$$

where $\mu_{i,j}^{\rm GZK}$ is the number of events in a bin of the energy–zenith angle plane predicted by the cosmogenic model and $\mu_{i,j}^{\alpha}$ is the value attributable to a generic astrophysical $E_\nu^{-\alpha}$ power-law flux. One important question is whether the observed data are consistent with the expectations from cosmogenic neutrino models [6] or a softer power-law flux, such as $E_\nu^{-2}$, as expected from astrophysical neutrinos. The test statistic here is

$$\Lambda = \log \frac{L_{\rm power}(\widehat{\lambda_\alpha})}{L_{\rm GZK}(\widehat{\lambda_{\rm GZK}})}, \tag{7}$$

where $\widehat{\lambda_\alpha}$ and $\widehat{\lambda_{\rm GZK}}$ maximize the likelihood functions.

### C. Calculations with astrophysical background

The astrophysical neutrino flux observed by IceCube indicates that contributions from a generic astrophysical power-law flux are expected in the PeV energy region [5]. We account for this possibility by introducing a nuisance flux in the form $\phi_\alpha = \kappa_\alpha E_\nu^{-\alpha}$, where $\kappa_\alpha$ is an arbitrarily chosen reference normalization. A small modification of Eq. (6) gives

$$L_{\rm GZK}(\lambda_{\rm GZK}, \lambda_\alpha) = \prod_{i,j} P(n_{i,j}; \lambda_{\rm GZK}\mu_{i,j}^{\rm GZK} + \lambda_\alpha \mu_{i,j}^{\alpha} + \mu_{i,j}^{\rm BG}). \tag{8}$$

Taking $\lambda_\alpha$ as a nuisance parameter, the likelihood ratio is constructed using the profile likelihood:

$$\Lambda(\lambda_{\rm GZK}) = \log \frac{L_{\rm GZK}(\widehat{\lambda_{\rm GZK}}, \widehat{\lambda_\alpha})}{L_{\rm GZK}(\lambda_{\rm GZK}, \widehat{\widehat{\lambda_\alpha}}(\lambda_{\rm GZK}))}, \tag{9}$$

where the double-hat notation represents the profiled value of the parameter $\lambda_\alpha$, defined as the value that maximizes $L_{\rm GZK}$ for the specified $\lambda_{\rm GZK}$. This likelihood ratio, in which $\lambda_{\rm GZK} = 1$, is the test statistic for a given cosmogenic neutrino model. The baseline model of the nuisance flux is built with $\alpha = 2$. The impact of different power-law indices is negligible when constraints are placed in the EHE region because we confirmed that upper limits of $\lambda_{\rm GZK}$ with various $\alpha$ ranging from 2.5 to 2.0 are completely consistent within the statistical precision of pseudoexperiments to produce a PDF of $\Lambda$. The recent model-dependent p-values and the upper limits for the selected cosmogenic models in Ref. [5] were obtained using this procedure.

### D. Extension to differential limit

The inclusion of an astrophysical nuisance parameter can be extended to the differential limit calculation. The differential limit at a neutrino energy of $E_\nu^c$ presented here is the limit for the flux of $\phi_{\rm diff} = \kappa_E E_\nu^{-1}$ ranging over an interval of one decade $[\log_{10}(E_\nu^c/{\rm GeV}) - 0.5, \log_{10}(E_\nu^c/{\rm GeV}) + 0.5]$. A generalized hypothesis test in the presence of an astrophysical flux can similarly be obtained with Eq. (8). Here, instead of using a cosmogenic model flux, $\phi_{\rm diff}$ is used. Thus,

$$L_{\rm diff}(\lambda_{\rm diff}, \lambda_\alpha) = \prod_{i,j} P(n_{i,j}; \lambda_{\rm diff}\mu_{i,j}^{\rm diff}(E_\nu^c) + \lambda_\alpha \mu_{i,j}^{\alpha} + \mu_{i,j}^{\rm BG}), \tag{10}$$

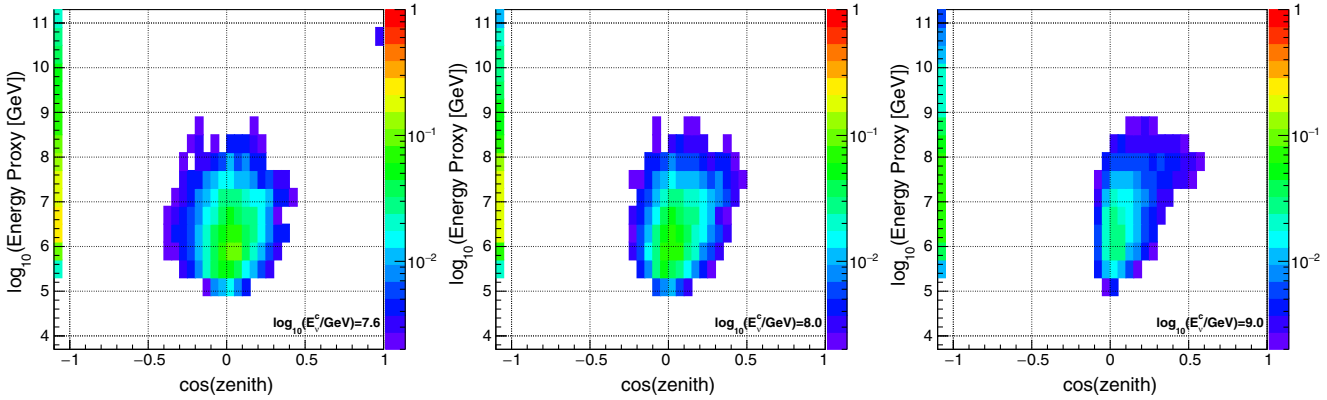


FIG. 4. Event distributions as functions of the energy proxy and cosine of the reconstructed zenith angle for the flux $\phi_{\rm diff} = \kappa_E E_\nu^{-1}$, spanning a one-decade energy interval centered at $E_\nu^c$. The event distributions include the contributions from all three neutrino flavors. Events classified as non-track-like are plotted in the bins of $\cos(\text{zenith}) = -1.1$. From left to right, the distributions for $\log_{10}(E_\nu^c/\text{GeV}) = 7.6$, 8.0, and 9.0 are shown. Note that this energy proxy was designed to work across all event topologies for the EHE analysis. Better energy estimates are obtained by dedicated energy reconstructions optimized for a specific event topology. For display purposes, the normalization $\kappa_E$ has been set here so the energy flux $E_\nu^2\phi_{\rm diff} = 1.0 \times 10^{-8}$ GeV/cm$^2$ sec sr at an energy of $E_\nu^c$.

where $\mu^{\rm diff}$ represents contributions from the flux $\phi_{\rm diff}$ with a one-decade energy interval centered at $E_\nu^c$. Thus, this expression is a function of $E_\nu^c$. Figure 4 presents the distribution of $\mu_{i,j}^{\rm diff}$ in the energy–zenith angle plane. The differences in the energy proxy between various $E_\nu^c$ are not substantial, because the deposited energy of a secondary muon track is only weakly correlated to the primary neutrino energy. This quality of resolution arises from the stochastic nature of the muon-energy-loss profile at PeV–EeV energies, the large variance in the fraction of neutrino energy channeling into muons, as well as variations in the position where muons are created. Instead, the zenith angle distribution exhibits more $E_\nu^c$ dependence. The larger the value of $E_\nu^c$, the more events are distributed above the horizon, where $\cos(\theta) \geq 0$. This occurs because neutrinos with higher energies experience stronger absorption effects during their propagation through the Earth. The zenith angle distribution is a key feature for setting the differential limit at energies higher than $10^7$ GeV.

The test statistic is constructed as

$$\Lambda(\lambda_{\rm diff}, E_\nu^c) = \log \frac{L_{\rm diff}(\lambda_{\rm diff}\widehat{(E_\nu^c)}, \widehat{\lambda_\alpha})}{L_{\rm diff}(\lambda_{\rm diff}(E_\nu^c), \widehat{\widehat{\lambda_\alpha}}(\lambda_{\rm diff}(E_\nu^c)))}. \quad (11)$$

An ensemble of pseudoexperiments is used to construct the PDF of $\Lambda(\lambda_{\rm diff}, E_\nu^c)$, and gives the upper limit of $\lambda_{\rm diff}$ at a given confidence level, for an energy of $E_\nu^c$. By repeating the same procedure with varying $E_\nu^c$, the differential upper limit as a function of neutrino energy is produced.

Figure 5 presents the distributions of the values of the negative log-likelihood $-\log L_{\rm diff}$ for several values of the

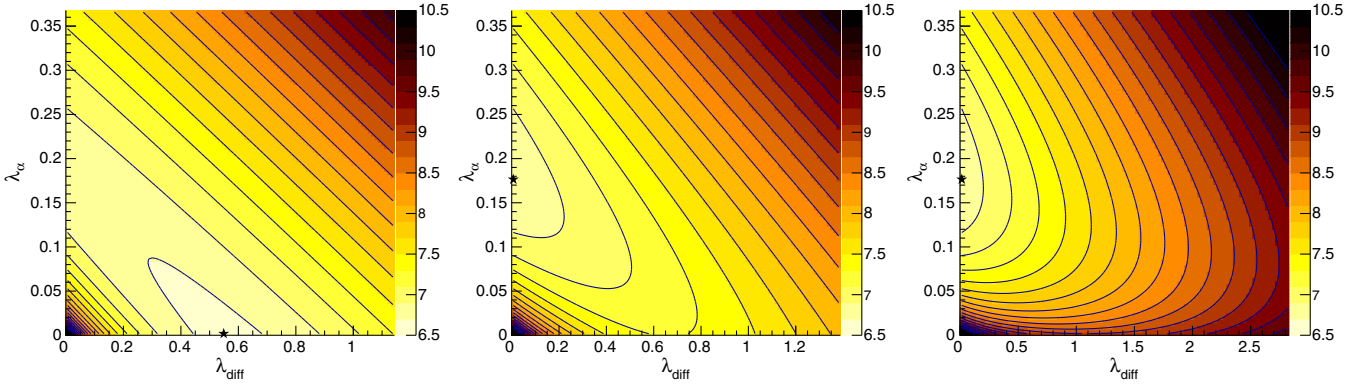


FIG. 5. Distribution of the negative log-likelihood ($-\log L_{\rm diff}$) for the hypothesis of $E_\nu^{-1}$ flux ranging over an energy interval of one decade, centered at $E_\nu^c$, on the $\lambda_{\rm diff}$-$\lambda_\alpha$ plane. Here $\lambda_{\rm diff}$ denotes the multiplier to the one-decade box-type spectrum $\phi_{\rm diff}$ and $\lambda_\alpha$ is the multiplier to the power-law nuisance spectrum $\phi_\alpha$ representing the astrophysical background. The star indicates the minimum on the $-\log L_{\rm diff}$ plane. From left to right, the distributions for $\log_{10}(E_\nu^c/\text{GeV}) = 7.6$, 8.0, and 9.0 are shown. These results are calculated using the nine-year set of IceCube data containing two PeV-energy events described in Sec. V. The power-law index of astrophysical flux, $\alpha$, is set to 2 in these examples.

neutrino energy $E_\nu^c$. The local minimum point on each of the $\lambda_{\rm diff}$-$\lambda_\alpha$ planes corresponds to $\widehat{\lambda_{\rm diff}(E_\nu^c)}$, $\widehat{\lambda_\alpha}$ that maximize the likelihood. At $E_\nu^c = 10^{7.6}$ GeV, the minimal point is found at $\lambda_\alpha = 0$, which implies that the observational data including the two detected events (see Sec. V) are attributed to $\phi_{\rm diff}$ centered at an energy of $10^{7.6}$ GeV, and do not require an astrophysical nuisance flux. This result occurs because the primary energies of the neutrinos initiating the detected events are likely to originate in the one-decade-energy interval of $\phi_{\rm diff}$. In the case of the central energy $E_\nu^c$ of $10^8$ GeV, $\lambda_{\rm diff} = 0$ maximizes the likelihood, implying that the data disfavor the one-decade box-type spectrum $\phi_{\rm diff}$ but prefer a nonzero component of the astrophysical nuisance flux. Further increases in the central energy $E_\nu^c$ weaken the correlation between $\lambda_\alpha$ and $\lambda_{\rm diff}$ and the upper limit of the one-decade box flux $\phi_{\rm diff}$ becomes less dependent on the intensity of the astrophysical nuisance flux, as one can see in the far-right plot of Fig. 5. Because the differential limit corresponds to the 90% C.L. upper limit of $\lambda_{\rm diff}$, this method gives the limit on $\phi_{\rm diff}$ in the presence of a possible astrophysical flux whose intensity $\lambda_\alpha$ is estimated by the real data sample. The estimated astrophysical neutrino intensity with $\alpha = 2$ is $E_\nu^2\phi_{\nu_e+\nu_\mu+\nu_\tau} = 1.7 \times 10^{-9}$ GeV/cm$^2$ sec sr regardless of $E_\nu^c$ when $E_\nu^c \gtrsim 5 \times 10^7$ GeV. The obtained limit is robust against the different assumptions about the astrophysical neutrino spectrum, such as a softer spectrum of $\alpha = 2.5$ or a spectral cutoff at 3 PeV as the resultant limit changes only by $\lesssim$5% with these various spectral assumptions.

For the previously published differential EHE limit [5], no nuisance parameter was used to account for an astrophysical background neutrino flux and the limit applies to the total neutrino flux over a decade in energy. Employing the astrophysical nuisance parameter in the calculation of the differential limit, one must consider that the PDF of the test statistic $\Lambda$, given by Eq. (11), depends on the true value of the multiplier for the astrophysical flux in contrast to the consequence of the widely used Wilks' theorem for high statistical data samples. It implies that the resultant limit may depend on the nuisance flux multiplier $\lambda_\alpha$, whose true value is yet to be understood. For setting the differential limit, we calculated the PDF of the test statistic $\Lambda$ by pseudoexperiments with various astrophysical flux intensities and found that the case of no astrophysical background resulted in the most conservative limit. Though the likelihood function and test statistic do include the nuisance astrophysical flux as a floating parameter [see Eq. (11)], the differential limit presented here is, hence, derived by the $\Lambda$ distribution assuming no astrophysical flux.

## V. RESULTS AND DISCUSSION

Two events passing the final selection criteria were observed; one event was reported in the previous analyses [5,29], and the newly found event in the additional two-year sample was detected in December 2016. It appears as a partially contained shower event. The energy proxy of this event used in the present analysis ($E_{\rm proxy}$) is 2.7 PeV. Note that the best-estimated energy of this uncontained shower event is different from the energy proxy value. A dedicated energy loss reconstruction algorithm based on extensive simulations of this type of event estimate its energy as 5.9 PeV. Additional details will be published elsewhere. The characteristics of the observed events are listed in Table II.

The hypothesis that these two events are backgrounds of atmospheric origin was tested by the likelihood ratio test statistic of Eq. (5) with $\lambda = 0$ and is rejected with a p-value of 0.024% ($3.5\sigma$). They are found compatible with a generic astrophysical $E^{-2}$ power-law flux with a p-value of 78.8%, whereas they are inconsistent with the cosmogenic hypothesis with a p-value of 2.5% ($2.0\sigma$), calculated using the test statistic of Eq. (7) employing the GZK neutrino model by Ahlers *et al.* [24]. The two observed events are more consistent with neutrinos from astrophysical power-law flux extending from TeV to PeV energies than from the cosmogenic flux peaking at energies in the EeV range.

The systematic uncertainties are the same as in the previous analysis [5] and each of the sources of systematic errors is fully described in Ref. [3]. The upper limits are weakened primarily by a potential NPE shift due to uncertainties in the detector's optical detection efficiency, and potential signal reduction due to uncertainties in the neutrino-nucleon cross section. Differential limits are derived including the worst-case combinations of these uncertainties. The effective softening of the limit was by about 28% below $4 \times 10^8$ GeV and by about 11% at about $10^9$ GeV and above.

Figure 6 presents the differential upper limit on the all-flavor neutrino flux using this new method based on the nine-year sample of IceCube data. The two observed events

TABLE II. Characteristics of the detected events found in this analysis. The energy proxy values listed here represent the estimates of energy deposition that are used for building the binned Poisson likelihood in the present analysis. They are obtained by the event reconstruction designed to be applicable to the EHE event sample regardless of their event topology. The best-estimated $\nu$ energy displays the parent neutrino energy estimates obtained by dedicated event reconstructions optimized for each event topology.

| | Energy proxy in the present analysis [PeV] | Best estimated $\nu$ energy [PeV] | Event topology |
|---|---|---|---|
| Event 1 | 2.6 | 8.7 (median [29]) | Track |
| Event 2 | 2.7 | 5.9 | Uncontained shower |

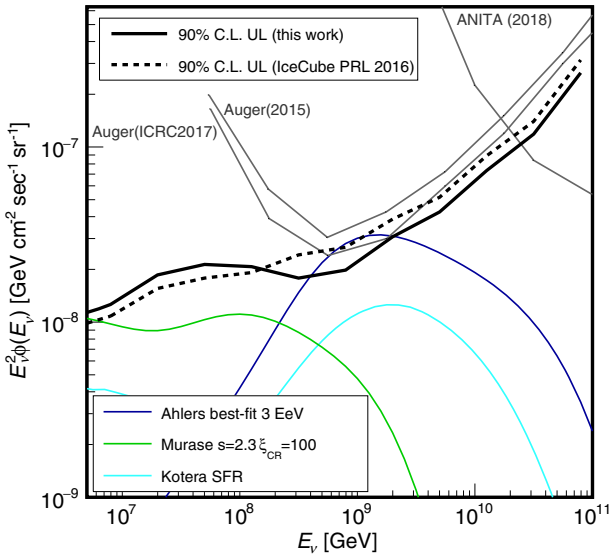


FIG. 6. All-flavor differential 90% C.L. upper limit based on the nine-year sample of IceCube data (solid line). Cosmogenic neutrino model predictions (assuming primary protons) by Kotera *et al.* [8] and Ahlers *et al.* [24], and an astrophysical neutrino model by Murase *et al.* [30] are shown for comparison. Differential limits for one-energy-decade $E_\nu^{-1}$ flux by other experiments are also shown for Auger (2015) [4], (ICRC2017) [10], and ANITA [31] with appropriate normalization by considering the energy bin width and neutrino flavor. The previous IceCube limit from the analysis of seven years of data [5] with the similar likelihood ratio framework but without a nuisance astrophysical background flux parameter is also shown for reference (dashed line).

weaken the limit below $4 \times 10^8$ GeV, while the limit becomes more stringent at higher energies as the astrophysical background completely accounts for the detected events. In the energy range most relevant to UHECR emissions, the present limit is stronger than the previous IceCube limit [5] even though the number of events remaining in the final data sample has doubled from one event to two. The new method for calculating differential upper limits with the nuisance flux strengthens the limit by ~45 % in the energy region around $10^9$ GeV in addition to the statistical improvements by adding two years of data. The limit applies to the constraints of the EHE cosmic neutrino flux on top of a power-law flux of astrophysical neutrinos. Any departure from $\alpha = 2$ in the nuisance $\phi_\alpha$ model has a very minimal impact on the obtained limit, especially at energies of $3 \times 10^8$ GeV or higher, the main energy region of interest for this study. The presented limit is also insensitive to systematic uncertainties in the energy proxy and topology of the detected events.

The presented differential upper limit in the energy region between $5 \times 10^6$ and $2 \times 10^{10}$ GeV is the most constraining model-independent upper limit currently reported. Models predicting a flux of $E_\nu^2 \phi_{\nu_e+\nu_\mu+\nu_\tau} \simeq 2 \times 10^{-8}$ GeV/cm$^2$ sec sr at $10^9$ GeV are disfavored by the IceCube observations. Although the newly detected PeV-energy neutrino event relaxed the present limit below $4 \times 10^8$ GeV, the obtained differential limit represents our most recent model-independent bound given by large IceCube exposure.

The present limit constrains a significant portion of the parameter space in EHE neutrino models that assume a proton-dominated UHECR composition. This constraint arises because the energy flux of UHECRs at 10 EeV, about $2 \times 10^{-8}$ GeV/cm$^2$ sec sr, is comparable to the present neutrino differential limit. The UHECR flux is contributed only from sources in the local Universe within a distance of $R_{\mathrm{GZK}} \sim 100$ Mpc because of the energy attenuation of UHECR protons colliding with the cosmic microwave background. However, neutrinos are able to travel cosmological distances of $O(c/H_0) \sim 4$ Gpc. Thus, UHECR sources within a sphere of about $c/H_0$ contribute to the expected neutrino flux. This volume effect generally increases the neutrino flux relative to the UHECR flux by a factor of about $c/H_0/R_{\mathrm{GZK}} \sim O(10)$. This balances the energy conversion factor from a UHECR proton to its daughter neutrino (5–10%), leading to an amount of neutrino energy flux comparable to the energy flux of UHECRs, if the observed UHECRs are protons, independent of the details of the neutrino production model. The present improved limit above $10^8$ GeV on the proton-dominated UHECR composition model is, therefore, robust against theoretical and observational uncertainties such as the cosmogenic neutrino intensity at PeV energies, which is determined by the extragalactic background light whose intensity is still uncertain [32]. Constrained by the differential limit, the interaction model-independent constraints [33] can be applied to the UHECR transition/composition models such as the proton dip model [34].

While the differential upper limits provide a good indicator of how the bound of EHE neutrino flux constrains different models, the model- *dependent* upper limits are more stringent in constraining each model. This arises because the EHE neutrino models, in general, predict neutrino fluxes ranging across several decades of neutrino energy. This behavior is demonstrated by the fact that the cosmogenic neutrino flux reported by Kotera *et al.* [8] and the active galactic nuclei (AGN) neutrino flux reported by Murase *et al.* [30], as shown in Fig. 6, were disfavored in this analysis. Table III presents the results of the model-dependent tests for selected cosmogenic models and an astrophysical AGN model. These constraints were obtained by following the procedure described in Sec. IV C and are compatible with the analysis based on the seven-year set of IceCube data [5] though the newly detected PeV-energy event slightly weakens the constraints.

TABLE III. Neutrino model tests: Expected number of events, p-values from the model hypothesis test, and 90% C.L. model-dependent limits in terms of the model rejection factor (MRF) [25], defined as the ratio between the flux upper limit and the predicted flux. The systematic uncertainties are taken into account in setting the MRFs and the errors on p-values. All of the models listed here assume proton-dominated UHECRs, except for the AGN model by Murase *et al* where the baryon loading factor $\xi_{\rm CR} = 100$ so that the injected cosmic rays from the blazars can achieve the observed UHECR generation rate around $10^{10}$–$10^{10.5}$ GeV.

| $\nu$ Model | Event rate | p-value | MRF |
|---|---|---|---|
| Kotera *et al.* [8] | | | |
| SFR | 4.8 | $13.3^{+6.5}_{-2.3}\%$ | 1.23 |
| Ahlers *et al.* [24] | | | |
| best fit, 1 EeV | 3.7 | $19.2^{+13.2}_{-3.2}\%$ | 1.51 |
| Ahlers *et al.* [24] | | | |
| best fit, 3 EeV | 5.7 | $4.6^{+2.6}_{-2.0}\%$ | 0.68 |
| Ahlers *et al.* [24] | | | |
| best fit, 10 EeV | 7.0 | $1.8^{+4.1}_{-0.5}\%$ | 0.63 |
| Aloisio *et al.* [35] | | | |
| SFR | 6.3 | $4.1^{+7.7}_{-0.9}\%$ | 0.93 |
| Murase *et al.* [30] | | | |
| AGN, $s = 2.3$, $\xi_{\rm CR} = 100$ | 9.9 | $1.5^{+6.7}_{-1.0}\%$ | 0.74 |

## VI. SUMMARY

In this study, an EHE neutrino search using a nine-year IceCube data set was conducted, and we identified two distinct events with energies beyond 1 PeV. No events in the energy region above 10 PeV were found. This observation indicates that no neutrinos were induced by UHECR nucleons via the GZK mechanisms. This is consistent with the model-dependent constraints previously published [5] based on the seven years of data. It can be concluded that the cosmological evolution of UHECR sources must be comparable to or weaker than the star formation rate, a generic measure of structure formation history in the Universe [36], if the mass composition of UHECRs is proton-dominated. This finding is also consistent with the constraints from the diffuse extragalactic $\gamma$-ray background [37,38] measured by Fermi-LAT [39].

In order to place an EHE neutrino flux limit with the present IceCube data set containing astrophysical neutrino background events, we introduced a new method that employs a binned Poisson likelihood method with a nuisance parameter to represent the TeV–PeV energy astrophysical neutrino flux. The intensity of the nuisance flux is determined from the observed data using a profile likelihood construction. The obtained differential limit is the most stringent recorded to date in the energy range between $5 \times 10^6$ and $2 \times 10^{10}$ GeV. This indicates that any cosmic neutrino model predicting a three-flavor neutrino flux of $E_\nu^2 \phi_{\nu_e+\nu_\mu+\nu_\tau} \simeq 2 \times 10^{-8}$ GeV/cm$^2$ sec sr at $10^9$ GeV is severely constrained. This is a universal bound of EHE cosmic neutrinos, regardless of the model of the EHE neutrino production and their sources.

The present limits with IceCube observations significantly challenge the most popular candidates for UHECR sources, such as $\gamma$-ray bursts and radio-loud AGNs, but if the highest-energy cosmic rays are not proton-dominated, it is clear that these constraints are weakened. A mixed-composition scenario, in general, predicts EHE neutrinos with an intensity lower than the present bound by an order of magnitude [38]. A larger-scale neutrino detector is required to measure the EHE neutrino flux in this case. Experimental constraints on sources of UHECRs of mixed or heavy composition will be provided in a next-generation detector such as ARA [40], ARIANNA [41], or IceCube-Gen2 [42].

## ACKNOWLEDGMENTS

The IceCube Collaboration designed, constructed and now operates the IceCube Neutrino Observatory. Data processing and calibration, Monte Carlo simulations of the detector and of theoretical models, and data analyses were performed by a large number of collaboration members, who also discussed and approved the scientific results presented here. The main author of this manuscript was Shigeru Yoshida. It was reviewed by the entire collaboration before publication, and all authors approved the final version of the manuscript.

We acknowledge the support from the following agencies: USA—U.S. National Science Foundation-Office of Polar Programs, U.S. National Science Foundation-Physics Division, Wisconsin Alumni Research Foundation, Center for High Throughput Computing (CHTC) at the University of Wisconsin-Madison, Open Science Grid (OSG), Extreme Science and Engineering Discovery Environment (XSEDE), U.S. Department of Energy-National Energy Research Scientific Computing Center, Particle astrophysics research computing center at the University of Maryland, Institute for Cyber-Enabled Research at Michigan State University, and Astroparticle physics computational facility at Marquette University; Belgium—Funds for Scientific Research (FRS-FNRS and FWO), FWO Odysseus and Big Science programmes, and Belgian Federal Science Policy Office (BELSPO); Germany—Bundesministerium für Bildung und Forschung (BMBF), Deutsche Forschungsgemeinschaft (DFG), Helmholtz Alliance for Astroparticle Physics (HAP), Initiative and Networking Fund of the Helmholtz Association, Deutsches Elektronen Synchrotron (DESY), and High Performance Computing cluster of the RWTH Aachen; Sweden—Swedish Research Council, Swedish Polar Research Secretariat, Swedish National Infrastructure for Computing (SNIC), and Knut and Alice Wallenberg Foundation; Australia—Australian Research Council; Canada—Natural Sciences and Engineering Research Council of Canada, Calcul Québec, Compute Ontario,

Canada Foundation for Innovation, WestGrid, and Compute Canada; Denmark—Villum Fonden, Danish National Research Foundation (DNRF); New Zealand—Marsden Fund; Japan—Japan Society for Promotion of Science (JSPS) and Institute for Global Prominent Research (IGPR) of Chiba University; Korea—National Research Foundation of Korea (NRF); Switzerland—Swiss National Science Foundation (SNSF).

[1] A. Aab *et al.* (Pierre Auger Collaboration), Science **357**, 1266 (2017).
[2] R. Abbasi *et al.* (IceCube Collaboration), Phys. Rev. D **83**, 092003 (2011).
[3] M. G. Aartsen *et al.* (IceCube Collaboration), Phys. Rev. D **88**, 112008 (2013).
[4] A. Aab *et al.* (Pierre Auger Collaboration), Phys. Rev. D **91**, 092008 (2015).
[5] M. G. Aartsen *et al.* (IceCube Collaboration), Phys. Rev. Lett. **117**, 241101 (2016); **119**, 259902 (2017).
[6] V. S. Berezinsky and G. T. Zatsepin, Phys. Lett. B **28**, 423 (1969).
[7] S. Yoshida and A. Ishihara, Phys. Rev. D **85**, 063002 (2012).
[8] K. Kotera, D. Allard, and A. V. Olinto, J. Cosmol. Astropart. Phys. 10 (2010) 013.
[9] G. Decerprit and D. Allard, Astron. Astrophys. **535**, A66 (2011).
[10] Pierre Auger Collaboration, Proc. Sci. ICRC2017 (**2017**) 972.
[11] L. A. Anchordoqui, J. L. Feng, H. Goldberg, and A. D. Shapere, Phys. Rev. D **66**, 103002 (2002).
[12] G. J. Feldman and R. D. Cousins, Phys. Rev. D **57**, 3873 (1998).
[13] M. G. Aartsen *et al.* (IceCube Collaboration), Phys. Rev. Lett. **111**, 021103 (2013).
[14] M. G. Aartsen *et al.* (IceCube Collaboration), J. Instrum. **12**, P03012 (2017).
[15] D. Heck *et al.*, Forschungszentrum Karlsruhe, 1998, Report No. FZKA 6019.
[16] E.-J. Ahn, R. Engel, T. K. Gaisser, P. Lipari, and T. Stanev, Phys. Rev. D **80**, 094003 (2009).
[17] A. Gazizov and M. P. Kowalski, Comput. Phys. Commun. **172**, 203 (2005).
[18] R. Enberg, M. H. Reno, and I. Sarcevic, Phys. Rev. D **78**, 043005 (2008).
[19] A. Bhattacharya, R. Enberg, Y. S. Jeong, C. S. Kim, M. H. Reno, I. Sarcevic, and A. Stasto, J. High Energy Phys. 11 (2016) 167; R. Gauld, J. Rojo, L. Rottoli, S. Sarkar, and J. Talbert, J. High Energy Phys. 02 (2016) 130.
[20] S. Yoshida, R. Ishibashi, and H. Miyamoto, Phys. Rev. D **69**, 103004 (2004).
[21] R. Abbasi *et al.* (IceCube Collaboration), Phys. Rev. D **82**, 072003 (2010).
[22] M. G. Aartsen *et al.* (IceCube Collaboration), Nucl. Instrum. Methods Phys. Res., Sect. A **736**, 143 (2014).
[23] M. G. Aartsen *et al.* (IceCube Collaboration), Astropart. Phys. **92**, 30 (2017).
[24] M. Ahlers, L. A. Anchordoqui, M. C. Gonzalez–Garcia, F. Halzen, and S. Sarkar, Astropart. Phys. **34**, 106 (2010).
[25] G. Hill and K. Rawlins, Astropart. Phys. **19**, 393 (2003).
[26] M. G. Aartsen *et al.* (IceCube Collaboration), Phys. Rev. Lett. **113**, 101101 (2014).
[27] M. G. Aartsen *et al.* (IceCube Collaboration), J. Instrum. **9**, P03009 (2014).
[28] J. Ahrens *et al.* (AMANDA Collaboration), Nucl. Instrum. Methods Phys. Res., Sect. A **524**, 169 (2004).
[29] M. G. Aartsen *et al.* (IceCube Collaboration), Astrophys. J. **833**, 3 (2016).
[30] K. Murase, Y. Inoue, and C. D. Dermer, Phys. Rev. D **90**, 023007 (2014).
[31] P. W. Gorham *et al.* (ANITA Collaboration), Phys. Rev. D **98**, 022001 (2018).
[32] K. Mattila, P. Väisänen, K. Lehtinen, G. von Appen-Schnur, and Ch. Leinert, Mon. Not. R. Astron. Soc. **470**, 2152 (2017).
[33] J. Heinze, D. Boncioli, M. Bustamante, and W. Winter, Astrophys. J. **825**, 122 (2016).
[34] V. Berezinsky, A. Gazizov, and S. Grigorieva, Phys. Rev. D **74**, 043005 (2006).
[35] R. Aloisio, D. Boncioli, A. di Matteo, A. F. Grillo, S. Petrera, and F. Salamida, J. Cosmol. Astropart. Phys. 10 (2015) 006.
[36] A. M. Hopkins and J. F. Beacom, Astrophys. J. **651**, 142 (2006); H. Yüksel, M. D. Kistler, J. F. Beacom, and A. M. Hopkins, Astrophys. J. Lett. **683**, L5 (2008).
[37] V. Berezinsky, A. Gazizov, M. Kachelrieß, and S. Ostapchenko, Phys. Lett. B **695**, 13 (2011); V. Berezinsky, A. Gazizov, and O. Kalashev, Astropart. Phys. **84**, 52 (2016).
[38] N. Globus, D. Allard, E. Parizot, and T. Piran, Astrophys. J. **839**, L22 (2017).
[39] M. Ackermann *et al.* (Fermi-LAT Collaboration), Astrophys. J. **799**, 86 (2015).
[40] P. Allison *et al.* (ARA Collaboration), Phys. Rev. D **93**, 082003 (2016).
[41] S. W. Barwick *et al.* (ARIANNA Collaboration), Astropart. Phys. **70**, 12 (2015).
[42] IceCube collaboration, Proc. Sci. ICRC2017 (**2017**) 991.